Acousto-optical imaging using a powerful long pulse laser

Rousseau, Guy; Blouin, Alain; Monchalin, Jean-Pierre

Acousto-optical imaging using a powerful long pulse laser

Guy Rousseau*, Alain Blouin and Jean-Pierre Monchalin
Industrial Material Institute, National Research Council Canada,
75 de Mortagne Blvd, Boucherville, Québec, Canada, J4B 6Y4

ABSTRACT

Acousto-optical imaging is an emerging biodiagnostic technique which provides an optical spectroscopic signature and a spatial localization of an optically absorbing target embedded in a strongly scattering medium. The transverse resolution of the technique is determined by the lateral extent of ultrasound beam focal zone while the axial resolution is obtained by using short ultrasound pulses. Although very promising for medical diagnostic, the practical application of this technique is presently limited by its poor sensitivity. Moreover, any method to enhance the signal-to-noise ratio must obviously satisfy the in vivo safety limits regarding the acceptable power level of both the ultrasonic pressure wave and the laser beam. In this paper, we propose to improve the sensitivity by using a pulsed single-frequency laser source to raise the optical peak power applied to the scattering medium and to collect more ultrasonically tagged photons. Such a laser source also allows illuminating the tissues mainly during the transit time of the ultrasonic wave to maintain the average optical power below the maximum permissible exposure. In our experiment, a single-frequency Nd:YAG laser emitting 500-μs pulses with a peak power superior to 100 W was used. Photons were tagged in few-cm thick optical phantoms with tone bursts generated by an ultrasonic transducer. Tagged photons were detected with a GaAs photorefractive interferometer characterized by a large optical etendue to process simultaneously a large number of speckle grains. When pumped by high intensity laser pulses, such an interferometer also provides the fast response time essential to obtain an apparatus insensitive to the speckle decorrelation due to mechanical vibrations or tissues movements. The use of a powerful long pulse laser appears promising to enhance the signal level in ultrasound modulated optical imaging. When combined with a photorefractive interferometer of large optical etendue, such a source could allow obtaining both the sensitivity and the fast response time necessary for biodiagnostic applications.

Keywords: acousto-optical imaging, ultrasound-modulated optical imaging, acousto-optical tomography, ultrasonic photon tagging, ultrasound-tagged photons, photorefractive interferometer

1. INTRODUCTION

Optical imaging techniques for biomedical diagnostics are currently very actively developed. These techniques have in particular the advantage of being based on non-ionizing radiation and to be able to provide morphological as well as functional information.[1] Acousto-optical imaging (AOI) is an emerging technique which allows the localization of an optically absorbing target imbedded in a diffusive medium through the detection of ultrasound-modulated photons.[2-7] This method combines the good spatial resolution (mm scale) and penetration depth (cm scale) of ultrasound waves with the spectroscopic information provided by photons. A practical limit to the use of this technique is its poor sensitivity or low signal-to-noise ratio. Even though the optical absorption of water is relatively low in the therapeutic window, the strong scattering of photons propagating in tissues reduces significantly the number of collectable photons. Moreover, for biomedical applications, safety considerations limit the power level of both the ultrasonic wave and the laser beam. The peak negative pressure of the ultrasonic wave must remain below a value prescribed by the so-called mechanical index (MI) to avoid cavitation and its side effects.[8] Similarly, the laser beam irradiance must be maintained below the maximum permissible exposure (MPE) to avoid heating damage.[9] In acousto-optical imaging, the ultrasound-tagged photons can be detected by full field imaging of the speckle pattern with an array of detectors[3-4] (CCD camera) or by an interferometric scheme using a single photodetector.[2,5-7] Methods based on arrays of detectors require intensive data

* guy.rousseau@cnrc-nrc.gc.ca

processing but provide a better signal-to-noise ratio.[3-4] The interferometric scheme is either based on a confocal Fabry-Perot interferometer[5,10] or an adaptative photorefractive interferometer.[6-7,11] Both instruments present a large etendue (collecting power) when compared to conventional interferometers.[12] The adaptative photorefractive interferometer uses a photorefractive crystal to recombine the reference beam and the signal beam through a dynamic volume grating which replicates the wave front of the signal beam to that of the reference beam. This approach was developed for laser-ultrasonic non-destructive testing of materials where almost all the photons of the signal beam are modulated.[11] In acousto-optical imaging, most photons in the signal beam are not modulated since the insonified zone in the diffusive medium is generally much smaller than the illuminated zone. Moreover, an ultrasonic toneburst presents compression and rarefaction zones. Consequently, each scattered photon undergoes both positive and negative phase shifts, thereby acquiring a net phase modulation which is rather small.[13] A direct way to enhance the number of tagged photons is to increase the optical power incident on the diffusive medium. However, to respect the maximum permissible exposure in terms of average power, the increase of the instantaneous power must be counterbalanced by a reduction of the exposure duration. This suggests the use of a train of pulses of high peak intensity with an appropriate duty cycle. In such a situation, the number of photons is high mainly for the relevant period of time, that is, during the transit time of the ultrasonic toneburst in the diffusive medium. A laser pulse of high power density also shortens the response time of the dynamic hologram written in the crystal of the photorefractive interferometer. This is important to overcome the speckle decorrelation associated with mechanical vibrations and with tissue motions for *in vivo* applications. With a pulsed laser, a short response time is also essential to ensure the build-up of the dynamic hologram in a time shorter than the laser pulse duration.

2. EXPERIMENTAL SETUP

The schematic diagram of the experimental setup used for the acousto-optical measurements is shown in Fig. 1. The beam of the single-frequency laser source (L) is separated by a beam splitter (BS) into a reference beam (R) and a signal beam (S). The signal beam is directed (along the axis y) toward the diffusive medium (DM) which is locally insonified by an ultrasonic transducer (UT) emitting few-cycle acoustic pulses which propagate along the axis z. Photons collected at the output of the diffusive medium are sent together with the reference beam into a photorefractive interferometer (PRI) to detect the ultrasound-tagged photons as a function of time.

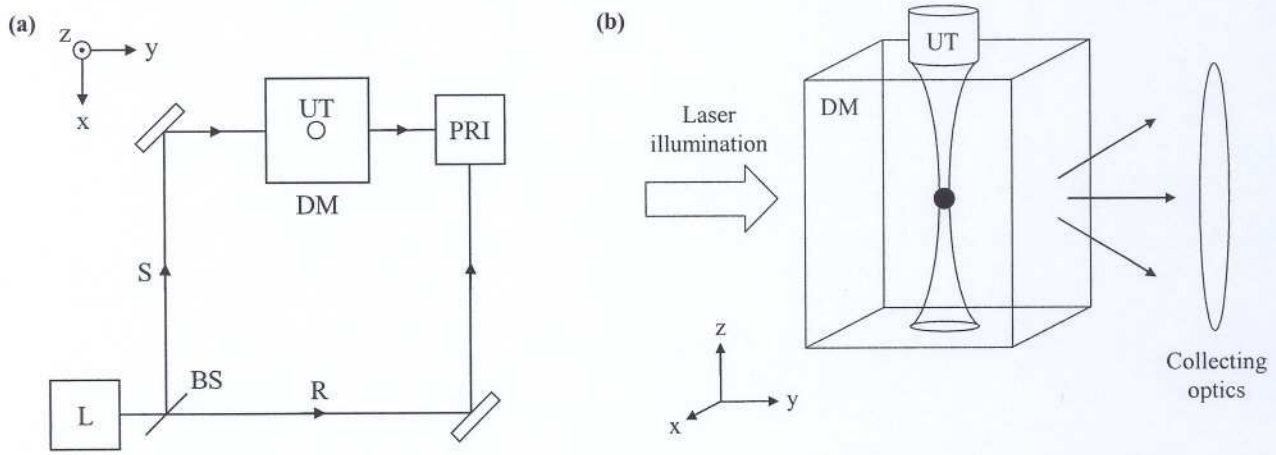

Figure 1 (a) Schematic setup of the acousto-optical imaging experiment. L: single-frequency laser source, BS: beam splitter, R: reference beam, S: signal beam, DM: diffusive medium, UT: ultrasonic transducer, PRI: photorefractive interferometer. **(b)** Geometry of the diffusive medium. The black sphere is an optically absorbing target.

Most results presented in the literature are obtained with low or moderate power single-frequency continuous-wave (cw) lasers of sufficiently long coherence length.[2-7] These sources limit the number of collectable photons at the exit of the diffusive medium. With photorefractive interferometers, low power cw laser sources also lengthen the response time of the photorefractive crystal which becomes vulnerable to the speckle decorrelation induced by mechanical vibrations or by motions within the diffusive medium (for *in vivo* applications). For biomedical applications, a direct power scaling is

not applicable since the maximum permissible exposure (MPE) in terms of average power is rapidly reached in the visible and the near infrared parts of the spectrum (from 0.2 W/cm^2 to 1.0 W/cm^2). Power scaling is still attractive when considering the low sensitivity of acousto-optical imaging methods due to a small tagged/untagged photons ratio and to the difficulty of collecting efficiently the scattered photons at the exit of the diffusive medium. An appropriate way to apply power scaling is the use of a source emitting a low duty cycle train of powerful laser pulses. Such a laser source can be obtained by amplifying a single-frequency cw laser beam with a flashlamp-pumped gain-switched amplifier. In the following subsections, we described the components of an AOI setup based on such a pulsed laser.

2.1 Pulsed laser source

In our experiment, a cw single-frequency laser beam of 200 mW at 1.064 μm is provided by a commercial Nd:YAG non planar ring oscillator. This master oscillator (MO) is followed by the gain-switched amplifier depicted in Fig. 2(a). The linearly polarized laser beam of the master oscillator is transmitted through a first optical isolator (OI1) to prevent feedback from the amplifier. The amplifier is composed of two Nd:YAG laser rods (LR1-2) pumped by a single flashlamp (FL) which is powered by a variable pulse width flashlamp controller. The first laser rod (LR1) is used as a two-pass amplifying medium. The counter-propagating beams are separated by a quarter-wave plate (QW) followed by a thin film polarizer (TFP). An optical isolator (OI2) located between the two laser rods prevents the self-oscillation of the amplifier. The third amplifying pass occurs in the second laser rod (LR2). In typical operating conditions, 530-μs (full width at half maximum) pulses of more than 280 mJ are obtained at a repetition rate of 25 Hz. Consequently, the overall gain, including the passive losses in the optical components, is higher than 2500. The gain in the third pass is typically around 5, indicating that gain saturation is almost reached. A typical pulse intensity profile at the output of the amplifier is shown in Fig. 2(b) where the peak power is higher than 500 W. Considering the repetition rate of 25 Hz, this corresponds to an average power of ~7 W.

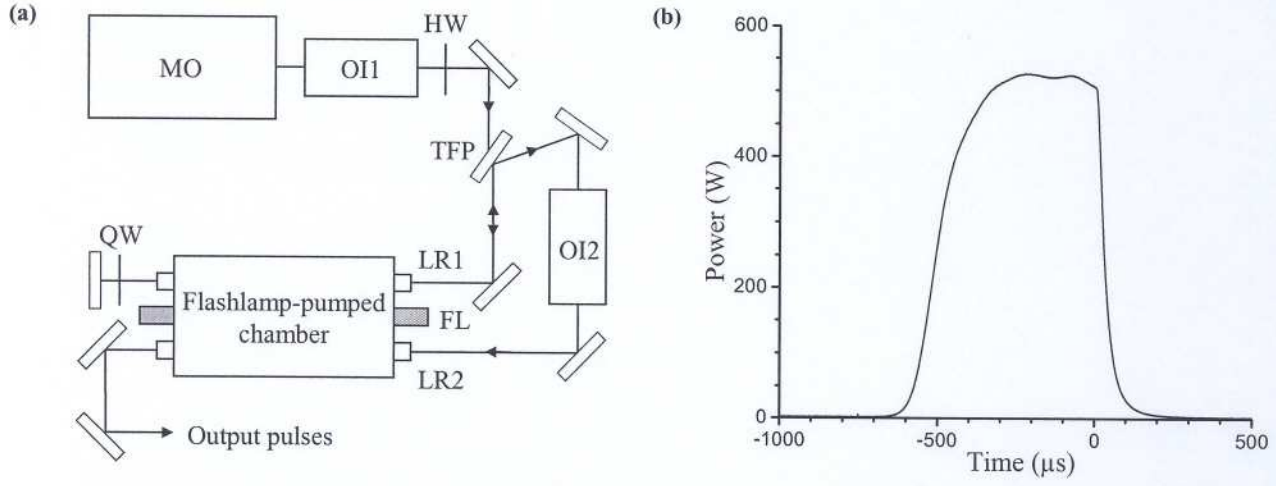

Figure 2 (a) Layout of the Nd:YAG pulsed amplifier. MO: 200-mW master oscillator, OI1-2: optical isolators, LR1-2: Nd:YAG laser rods (φ = 3 mm, L = 100 mm), FL: flashlamp, HW: half-wave plate, QW: quarter-wave plate, TFP: thin-film polarizer. Other components are plane dielectric mirrors **(b)** Typical output pulse intensity profile.

The use of counter-propagating orthogonal polarizations in the first laser rod minimizes the depolarization in the first two passes. The amplified output beam is partially depolarized by the thermal birefringence in the second laser rod of the amplifier. The output beam degree of polarization is typically around 0.8. The amplification process also gives rise to spatio-temporal inhomogeneities, that is, the temporal pulse intensity profile depends on the transverse position in the beam. This can be verified by simultaneously comparing the temporal intensity profile of the entire beam (integrated over its entire surface) with the temporal intensity profile of the same beam apertured by a diaphragm which cuts a significant part of the energy (80% in the case considered here). As it can be seen in Fig. 3(a), these intensity profiles can differ significantly. Such inhomogeneities can be minimized with a fiber-based mode scrambler (not shown). The beam of the amplifier is first coupled into a multimode step-index silica fiber (φ = 365 μm, NA = 0.22) with an f = 100 mm focusing lens. This fiber passes through a homemade mode scrambler composed of a vise with an appropriate jaw. By

applying a slight pressure with the vise, the micro bends of the fiber break its azimuthal symmetry and give rise to stress induced birefringence. This enhances the mode coupling and allows to filling the entire mode volume over a short length of fiber thereby homogenizing the spatio-temporal structure of the laser pulse. At the output of the mode scrambler, the intensity profile becomes much less sensitive to the presence of an aperture cutting a significant part of the energy. This can be seen in Fig. 3(b) where the apertured beam (upper curve) and the unapertured beam (lower curve) present the same intensity fluctuations. Such homogenization becomes important when a differential detection is used (see section 2.3) since the diffusive medium necessarily acts as an aperture on the signal beam whereas the reference beam is almost unapertured during its propagation. Consequently, the common-mode rejection ratio of the differential detector will be optimized only if the initial beam is homogenized. Another advantage of the laser beam homogenization is to obtain a more uniform illumination of the photorefractive crystal over the interaction volume between the reference and the signal beams. This ensures a more uniform response time within the interaction volume.

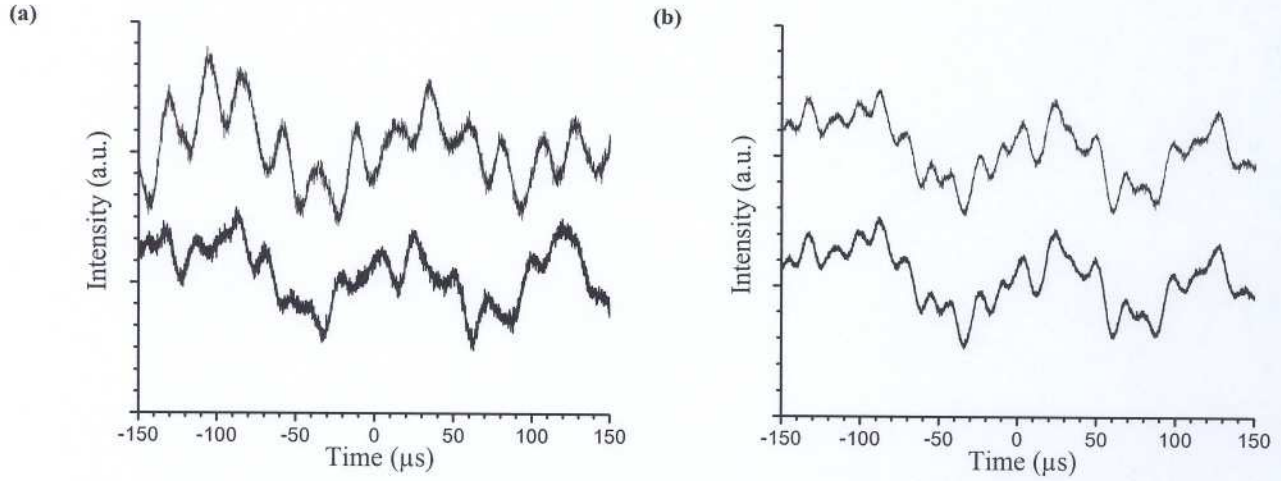

Figure 3 (a) Pulse intensity profiles with (upper curve) and without (lower curve) a circular aperture cutting 80% of the beam at the output of the amplifier (before the mode scrambler). **(b)** Pulse intensity profiles with (upper curve) and without (lower curve) a circular aperture cutting 80% of the beam at the output of the mode scrambler (beam homogenizer). In (a) and (b), the offset between both curves is arbitrary.

The spatio-temporal homogenization described above is a first way to reduce the impact of laser intensity noise when working in differential detection. However, even with the use of a mode scrambler and differential detection, residual low frequency noise components which are synchronized with the flashlamp are still observed at frequencies around 25, 42 and 65 kHz. These noise components are probably of thermo-acoustic origin (thermally excited acoustic resonance in the laser rods of the amplifier) and have an amplitude of the order of 0.1%. Since these noise components are synchronized with the pumping flashes, they become disturbing when the laser pulses are synchronized with the ultrasonic tonebursts. Moreover, the periods of these noise components are comparable to the duration of the tagged-photon signal. In order to minimize their effect when averaging data, it is useful to desynchronize the laser pulses and the ultrasonic tonebursts modulating the photons inside the diffusing medium. This is accomplished by adding a random variable delay between the laser pulses and the tonebursts. In the absence of synchronization with the laser pulses, the laser intensity noise components add incoherently and average to zero while the synchronization with the acoustic pulses ensures a coherent superposition of the tagged-photon signal. Such an artificial timing jitter acts as a "temporal scrambler" for the laser intensity noise.

2.2 Ultrasonic source and diffusive medium

The second part of the experimental setup is composed of the sample cell filled with milk as a diffusive medium and insonified by an ultrasonic transducer (see Fig. 1(b)). In our experiment, a 5-MHz transducer of 6.35 mm diameter was used. The transducer was typically fed with few-cycle sinusoidal tonebursts produced by an arbitrary waveform generator and amplified by a high power amplifier. The frequency of the toneburst was tuned at the specific resonance frequency of the transducer for optimal operation.

In a first step, the ultrasonic beam produced by the transducer was calibrated by using the setup shown in Fig. 4(a). In this setup, the ultrasonic transducer (UT) is immersed in water (W) and points toward the free water-air interface. Assuming that the particle displacement is essentially longitudinal (along the axis z) as for plane and slowly diverging pressure waves, the ultrasonic beam (UB) can be probed by measuring the displacement ξ_a of the water-air interface (as a function of time) with a broadband (10kHz - 35 MHz) heterodyne interferometer (HI) that uses the Fresnel reflection of the probe beam (PB) on the interface. The particles displacement ξ_w associated with the progressive wave propagating in water toward the free interface can be deduced from ξ_a with the relationship $\xi_a = \tau \xi_w$ where $\tau = 2Z_w/(Z_w + Z_a) \cong 2$ is the displacement transmission coefficient, $Z_w = 1.5 \times 10^{-3}$ Mrayl and $Z_a = 0.41 \times 10^{-3}$ Mrayl being the acoustic impedances of water and air. The pressure wave in water p_w is then calculated by numerically differentiating the measured curve ξ_a according to the relation $p_w = Z_w v_w$ where $v_w = \partial \xi_w / \partial t$ is the particle velocity in water.[14] When compared to hydrophone measurements, this method provides a high spatial resolution, a simple calibration and a broadband detection. A typical displacement waveform $\xi_a(t)$ obtained by this method is shown in Fig. 4(b) with the corresponding pressure waveform $p_w(t)$. The ultrasound field can be mapped without readjusting the probe beam by moving the transducer underneath the water with an xyz translation stage.

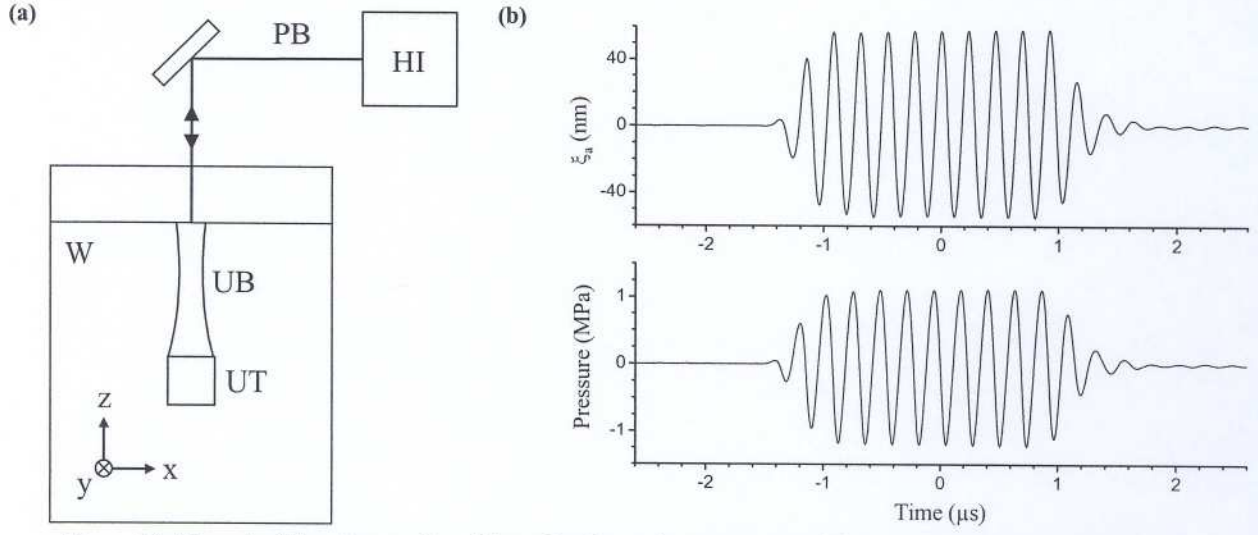

Figure 4 (a) Layout of the setup used to calibrate the ultrasonic pressure wave. W: water, UT: ultrasonic transducer, UB: ultrasonic beam, PB: probe beam, HI: heterodyne interferometer. **(b)** Typical calibrated displacement of the water-air interface and the corresponding ultrasonic pressure wave in water for a 10-cycle toneburst.

In our experiment, we have used undiluted milk (2%-fat homogenized milk) as a diffusive medium. The extinction coefficient μ_t of the milk sample was obtained by the collimated transmission method,[1] that is, by measuring the ballistic transmission of a 20-mm thick cell as a function of the milk concentration C in water. We have obtained $\mu_t = 5.99\,\text{mm}^{-1}$ from the fit with the relation $I(C) = I_0 \exp(-\mu_t TC)$ where T is the thickness of the cell. The Beer-Lambert absorption coefficient μ_a of water at 1.064 μm is found to be 1.44×10^{-2} mm^{-1}.[15-16] According to the relation $\mu_t = \mu_s + \mu_a$, the absorption of water is thus practically negligible in the determination of the scattering coefficient μ_s. Consequently, the scattering mean free path $l = \mu_s^{-1}$ of our milk sample was approximately 167 μm at a wavelength of 1.064 μm. This value is of the same order of magnitude than that of biological tissues at visible wavelength (100 μm). It should be noted, however, that the absorption coefficient of water is much higher at 1.064 μm than in the visible (~3.2×10^{-5} mm^{-1} at 532 nm) and in the near infrared (~2.0×10^{-3} mm^{-1} at 800 nm).[15-16]

2.3 Adaptative interferometer

The adaptative interferometer was based on a GaAs crystal (10 mm along the $<1\bar{1}0>$ axis by 7 mm along the $<001>$ axis). An energy transfer configuration in diffusion regime (no high voltage applied) was used. As shown in Fig. 5(a), the crystal is oriented so that both reference and signal beams enter the $(1\bar{1}0)$ face with TE polarizations. The angle Θ between the beams outside the crystal is approximately 70° which corresponds to a grating period of ~0.9 μm. The

grating vector $\vec{K}$ is oriented along the <001> axis for an optimal response. Special attention was paid to the optical etendue of the interferometer by using large numerical aperture aspherical lenses (EFL = 20 mm , NA = 0.54) and large area InGaAs photodetectors ($\varphi = 3$ mm). The optical etendue is determined by the surface S of the photodiodes (7 mm^2) and the numerical aperture of the aspherical lenses which corresponds to an acceptance solid angle Ω of approximately 1 sr. Consequently, the etendue of the interferometer is $E = S\Omega = 7\ mm^2$ sr. The slightly limiting component of the setup is the near infrared liquid light guide (LLG) with an etendue of 6.4 mm^2 sr. The layout of the photorefractive interferometer is shown in Fig. 5(b). The liquid light guide (3 mm core diameter, NA = 0.52) is used to carry the signal beam at the input of the interferometer. The diverging beam exiting from the LLG is then collimated with a first aspherical lens and polarized with a thin sheet polarizer. A second aspherical lens images the tip of the LLG on the entrance face of the GaAs crystal. The signal beam at the output of the crystal is then imaged on the photodetector 1 of the balanced receiver (BR) with two additional aspherical lenses. The diameter of the reference beam was adjusted to be similar to that of the signal beam (~3 mm) and to enter in the crystal with an angle of incidence of ~35°. The transmitted reference beam was then focused on the photodetector 2 of the balanced receiver after an appropriate attenuation with the variable attenuator (VA).

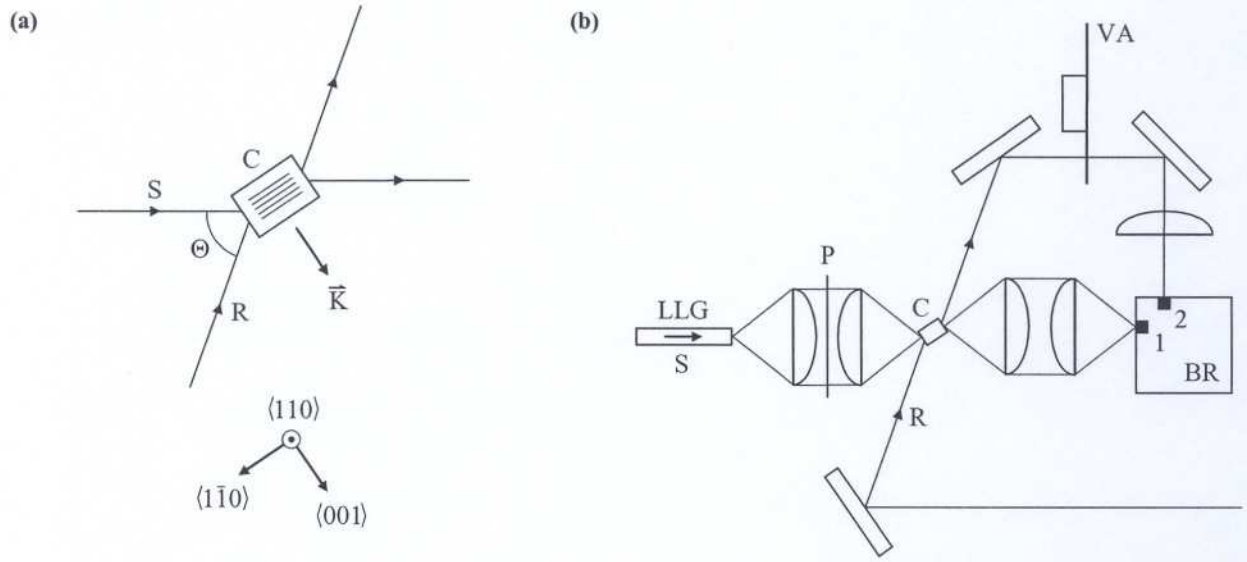

Figure 5 (a) Orientation of the photorefractive crystal. S: signal beam, R: reference beam, C: GaAs crystal, $\vec{K}$: grating vector. **(b)** Layout the photorefractive interferometer. LLG: liquid light guide, P: thin sheet polarizer, VA: variable attenuator, BR: balanced receiver using two InGaAs photodiodes (φ = 3 mm). Other components are plane dielectric mirrors and aspheric lenses (φ = 25 mm, f = 20 mm).

The crystal orientation used in this configuration leads to non-negligible reference beam diffusion and parasitic reflections which are in fact responsible for most of the energy impinging on the photodetector 1. This is due to the difficulty of collecting efficiently the signal beam photons at the exit of the diffusive medium. To minimize the DC component of the photocurrent generated by the photodetector 1, a second photodetector (photodetector 2 in Fig. 5(b)) was used in a differential configuration. The transmitted reference beam was directed toward this second photodetector and the variable attenuator was adjusted to balance the illumination on both detectors. This compensation of the optical illumination almost eliminates the DC photocurrent before its amplification by the transimpedance amplifier. The detection bandwidth was 7 MHz.

3. RESULTS

In our setup, the output beam of the amplifier was first homogenized with the fiber-based mode scrambler. Then, a variable beam splitter composed of a polarizing beam splitter cube and a half-wave plate was used to separate the reference and the signal beams. The reference beam exiting from the optical fiber of the mode scrambler was imaged with a magnification of 10 on the GaAs crystal (φ = 3.5 mm in the crystal). The signal beam was directed toward the

diffusive medium. The diameter of the signal beam impinging on the milk cell was typically of 20 mm. The outgoing photons were coupled in the photorefractive interferometer through a near infrared liquid light guide which was directly butted against the rear face of the milk cell (without any other collecting optics).

All the measurement were carried out in conditions allowed by the biomedical safety limits.[8-9] The mechanical index MI is given by the ratio $P/\sqrt{f}$ where P is the maximum negative pressure in MPa and f is the ultrasound frequency in MHz. According to this definition, the onset of cavitation in tissues occurs at $MI = 0.7$. Consequently, for biomedical applications, P must be maintained below 1.5 MPa at a frequency of 5 MHz. In our experiment, the maximum negative pressure was typically around 1.3 MPa. Moreover, at a wavelength of 1.064 μm, the laser beam irradiance must be maintained below a maximum permissible exposure (MPE) of 1.0 W/cm^2. In our experiment, the diffusive medium was typically illuminated on a 20-mm diameter surface with 100 mJ pulses at a repetition rate of 25 Hz. Consequently, the average irradiance was approximately of 0.8 W/cm^2.

All the measurements (at the exception of Fig. 8(a)) were obtained with a diffusive medium composed of undiluted milk (2%-fat homogenized milk) in a 20-mm thick cell. As it will be confirmed in section 3.2, this corresponds to a truly diffusive propagation regime with a ratio between the diffusive medium thickness (20 mm) and the scattering mean free path (167 μm) of approximately 120.

3.1 Properties of the tagged-photon signal

In the first step of the experiment, the tagged-photon signal was characterized as a function of the ultrasonic excitation of the diffusive medium without any absorbing target. With the energy transfer configuration considered here, a quadratic response with the optical phase modulation amplitude is expected. Figure 6(a) shows the tagged-photon signal as a function of time for different pressure wave amplitudes. These signals were obtained with 10-cycle tonebursts at 5 MHz. Figure 6(b) shows the corresponding maximums of the tagged-photon signals as a function of the amplitude of the driving voltage applied to the transducer (which is proportional to the pressure wave amplitude). As expected, the increase of the tagged-photon signal is quadratic with the amplitude of the pressure wave applied to the diffusive medium.

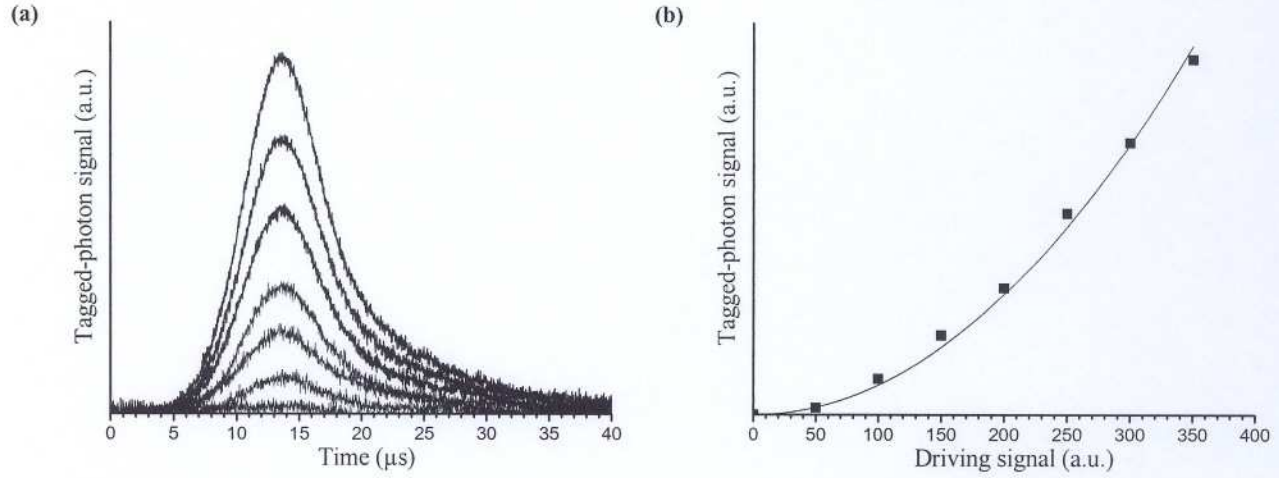

Figure 6 (a) Amplitude of the tagged-photon signal as a function of time obtained with 10-cycle tonebursts of different pressure wave amplitudes. **(b)** Corresponding maximum amplitudes of the tagged-photon signals as a function of the driving signal (before amplification) applied to the contact transducer.

The use of ultrasonic tonebursts provides an axial resolution (along the axis z) given by $\Delta z = c\Delta t$ where Δt is the duration of the toneburst and c is the speed of sound in the diffusive medium (~1.5 mm/μs in water-based media). With very short tonebursts (few cycles in the MHz frequency range), the spatial resolution along the ultrasonic axis z can be of the order of 1 mm. However, the insonified volume decreases linearly with the number of cycles which leads to a reduction of the tagged-photon signal.

Figure 7(a) shows the tagged-photon signal as a function of time by using pressure waves of the same amplitude but containing different number of acoustic cycles at 5 MHz. The curves correspond to the results obtained with 2^n acoustic cycles: n = 0 (1 cycle) for the lower curve, n = 7 (128 cycles) for the upper curve. Figure 7(b) shows the corresponding maximums of the tagged-photon signals as a function of the number of acoustic cycles. For a small number of acoustic cycles - corresponding to a pressure wave shorter than the zone probed by the collecting optics - the signal level increases almost linearly with the number of acoustic cycles. This behaviour is expected by the fact that the insonified volume also increases linearly with the number of acoustic cycles. This signal enhancement is however made at the cost of a lost of axial resolution along the axis z. A saturation of the signal level is reached when the ultrasonic toneburst duration correspond to a spatial extent (along the axis z) equal to or larger than the lateral extent of the volume probed by the collecting optics.

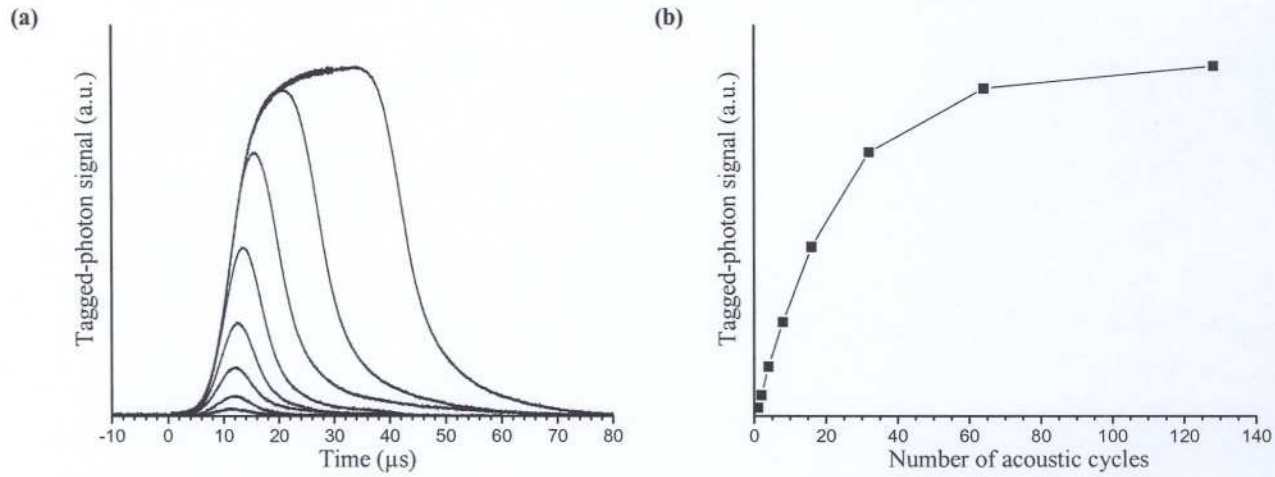

Figure 7 (a) Amplitude of the tagged-photon signal as a function of time obtained with tonebursts containing 2^n acoustic cycles (n = 0: lower curve, n = 7: upper curve). **(b)** Corresponding maximum amplitudes of the tagged-photon signals as a function of the number of acoustic cycles of the ultrasonic toneburst.

3.2 Absorbing target detection by AOI

Different propagation regimes exist from ballistic to diffusive. Since the evaluation of the scattering coefficient μ_s and the anisotropy factor g is not always straightforward, a simple test would be useful to verify whether the propagation regime is, for a given thickness of the diffusive medium, ballistic, diffusive or in-between. By definition, ballistic and quasi-ballistic (snake-like) photons cross the diffusive medium without significant deviation from their rectilinear path. Optical imaging is still applicable with these photons. A simple test to determine if the ballistic contribution is non-negligible consists in positioning the absorbing target in front of the diffusing medium within the incident laser beam. If the propagation is essentially ballistic, a local drop will be observed on the tagged-photon signal as a function of time. On the contrary, if the propagation is truly diffusive, the presence of a target in front of the diffusive medium will have no local effect but only an overall decrease of the tagged-photon signal. In the case of a diffusive propagation, a local drop of the signal will be observable only when the absorbing target is located within the insonified zone.

Examples of both propagation regimes are shown in Fig. 8. Figure 8(a) shows the results obtained with a 20-mm thick diffusive medium composed of 10% of milk and 90% of water (scattering mean free path of ~1.7 mm). A 2-cycle toneburst of 5 MHz was used in this case. The upper curve represents the tagged-photon signal observed without absorbing target. The signal obtained with a target (3-mm diameter black rubber cylinder aligned along the axis x) in front of the diffusive medium (middle curve) leads to a local drop of the signal level in a similar way to the presence of the same target within the insonified zone (lower curve). In this case, the ballistic contribution is non negligible and the local decrease of signal is essentially an optical shadow of the target. Moreover, the curves obtained with a target do not show any overall decrease of the signal when compared to the upper curve.

Figure 8(b) shows the results obtained with a diffusive medium composed of pure milk (20-mm thick cell, scattering mean free path of ~170 μm). A 10-cycle toneburst was used in this case. The presence of the target in front of the diffusive medium (middle curve) only leads to a global decrease of the signal level, indicating a truly diffusive propagation regime. A local decrease of the signal level is only observed when the target is located within the insonified zone (lower curve). It should be noted that curves in Fig. 8(b) were obtained by averaging only 32 consecutive sweeps.

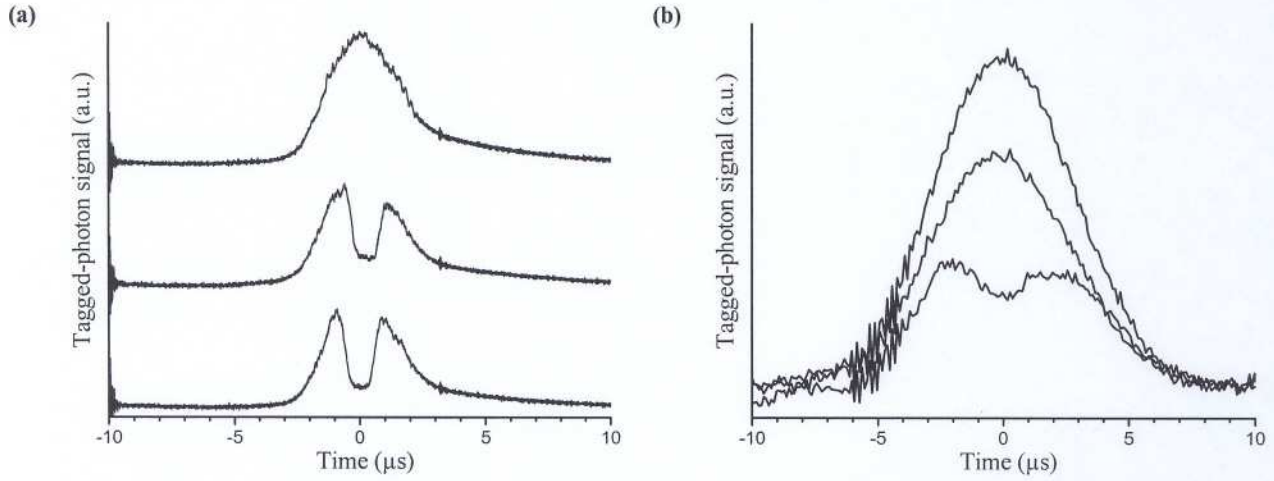

Figure 8 (a) Tagged-photon signals obtained with 2-cycle tonebursts using a 10% milk concentration diffusing medium of 20-mm thickness. Upper curve: without an absorbing target, middle curve: absorbing target in front of the diffusing medium, lower curve: absorbing target within the insonified zone. **(b)** Tagged-photon signals obtained with 10-cycle tonebursts using a 20-mm thick undiluted milk cell as a diffusing medium. Upper curve: no absorbing target, middle curve: absorbing target in front of the diffusing medium, lower curve: absorbing target within the insonified zone.

4. CONCLUSIONS

The work presented herein has shown that a pulsed laser source with a long coherence length can be implemented by using a flashlamp-pumped gain-switched amplifier at the output of a single-frequency cw laser. A low duty cycle pulse train with high peak power concentrates the illumination of the diffusive medium during the transit time of the acoustic pulse while maintaining the average power below the maximum permissible exposure. A high peak power also increases the available power density to reduce the response time of the dynamic hologram written in the photorefractive crystal. In the pulsed laser scheme considered here, a short response time is essential to write the grating in a timescale shorter than the laser pulse duration. In addition, a short response time also ensures to obtain a setup immune to mechanical vibrations and to the short speckle decorrelation time encountered *in vivo*.

We have used differential detection, variable delay synchronization and laser beam spatio-temporal homogenization to reduce the impact of the low frequency intensity noise encountered with the amplifier. The depolarization and the low frequency noise might be reduced by lowering the thermal impact of the pumping flashes in the Nd:YAG laser rods. This could be accomplished by pumping with diode lasers or by using larger rods with a lower gain. In the latter case, additional passes could be necessary to reach the same power level.

Adaptative two-wave interferometer based on a GaAs photorefractive crystal in energy transfer configuration was used to demodulate ultrasound-modulated photons. Special care was taken to increase the optical etendue of the interferometer by using large area InGaAs detectors and high numerical aperture aspherical lenses. The use of a liquid light guide has allowed an efficient collection of the scattered photons without limiting significantly the optical etendue of the setup. The use of a LLG allows a mechanical decoupling of the diffusive medium and the interferometer. It should be noted that the optical etendue of the interferometer could be increased further with commercially available components.

The spatial resolution along the ultrasound axis was obtained by the use of few-cycle tonebursts. Tagged-photon signals were obtained in a truly diffusive propagation regime without going beyond the biomedical safety limits in terms of ultrasonic wave amplitude and laser beam irradiance.

REFERENCES

1. L. V. Wang, H. Wu, *Biomedical Optics: Principles and Imaging*, John Wiley and Sons, Inc., Hoboken, New Jersey, 2007.
2. L. Wang, S. L. Jacques, and X. Zhao, "Continuous-wave ultrasonic modulation of scattered laser light to image objects in turbid media," Opt. Lett. **20**, 629-631 (1995).
3. S. Lévêque, A. C. Boccara, M. Lebec, and H. Saint-Jalmes, "Ultrasonic tagging of photon paths in scattering media: parallel speckle modulation processing," Opt. Lett. **24**, 181-183 (1999).
4. M. Atlan, B. C. Forget, F. Ramaz, A. C. Boccara, and M. Gross, "Pulsed acousto-optic imaging in dynamic scattering media with heterodyne parallel speckle detection," Opt. Lett. **30**, 1360-1362 (2005).
5. S. Sakadzic and L. V. Wang, "High-resolution ultrasound-modulated optical tomography in biological tissues," Opt. Lett. **29**, 2770-2772 (2004).
6. T. W. Murray, L. Sui, G. Maguluri, R. A. Roy, A. Nieva, F. Blonigen, and Ch. A. DiMarzio, "Detection of ultrasound-modulated photons in diffuse media using the photorefractive effect," Opt. Lett. **29**, 2509-2511, (2004).
7. F. Ramaz, B. C. Forget, M. Atlan, A. C. Boccara, M. Gross, P. Delaye, and G. Roosen, "Photorefractive detection of tagged photons in ultrasound modulated optical tomography of thick biological tissues," Opt. Express **12**, 5469-5474 (2004).
8. F. A. Duck, "Medical and non-medical protection standards for ultrasound and infrasound," Prog. biophys. molec. biol. **93**, 176-191 (2007).
9. Laser Institute of America, *American national standard for safe use of lasers* (ANSI Z136.1-2000), ANSI, Orlando, Florida, 2000.
10. J.-P. Monchalin, "Optical detection of ultrasound at a distance using a confocal Fabry-Perot interferometer," Appl. Phys. Lett. **47**, 14-16 (1985).
11. A. Blouin and J.-P. Monchalin, "Detection of ultrasonic motion of a scattering surface by two-wave mixing in a photorefractive GaAs crystal," Appl. Phys. Lett. **65**, 932-934 (1994).
12. J.-P. Monchalin, "Optical detection of ultrasound," IEEE Trans. Ultrason. Ferroelectr. Freq. Control **33**, 485-499 (1986).
13. L. V. Wang, "Mechanisms of Ultrasonic Modulation of Multiply Scattered Coherent Light: An Analytic Model," Phys. Rev. Lett. **87**, 043903 (2001).
14. L. E. Kinsler and A. R. Frey, *Fundamentals of Acoustics*, John Wiley and Sons, Inc., New York, 1962.
15. G. M. Hale and M. R. Querry, "Optical constants of water in the 200-nm to 200-μm wavelength region," Appl. Opt. **12**, 555-563 (1973).
16. S. Prahl, "Optical absorption of water," http://omlc.ogi.edu/spectra/water/